LAWRENCE
LIVERMORE
NATIONAL
LABORATORY

UCRL-JRNL-222153

A Monte Carlo Model for Interrogation of Thick Cargos for Clandestine Fissionable Materials; Tests with 14-MeV Neutrons

S.G. Prussin, M.-A. Descalle, J.M. Hall, J.A. Pruet, D.R. Slaughter, M.R. Accatino, O.J. Alford, S.J. Asztalos, A. Bernstein, J.A. Church, T. Gosnell, A. Loshak, N.W. Madden, D.R. Manatt, G.J. Mauger, A.W. Meyer, T.L. Moore, E.B. Norman, B.A. Pohl, D.C. Petersen, B. Rusnak, T.B. Sundsmo, W.K. Tembrook, R.S. Walling

June 16, 2006

Nuclear Instruments and Methods in Physical Research Section A: Accelerators,Spectrometers, Detectors and Associated Equipment

A Monte Carlo Model for Interrogation of Thick Cargos for Clandestine Fissionable Materials; Tests with 14-MeV Neutrons

by

S.G. Prussin[1*], M-A. Descalle, J.M. Hall, J.A. Pruet, D.R. Slaughter, M.R. Accatino, O.J. Alford, S. J. Asztalos, A. Bernstein, J.A. Church, T. Gosnell, A. Loshak, N.W. Madden, D.R. Manatt, G.J. Mauger, A.W. Meyer, T.L. Moore, E.B. Norman, B.A. Pohl, D.C. Petersen[1], B. Rusnak, T.B. Sundsmo, W.K. Tembrook and R.S. Walling, Lawrence Livermore National Laboratory, 7000 East Avenue • Livermore, CA 94550

Keywords: Cargo screening; Active interrogation; Neutron source; Fission product γ radiation

Abstract

A Monte Carlo model has been developed for interrogation of fissionable material embedded in thick cargos when high-energy β-delayed γ rays are detected following neutron-induced fission. The model includes the principal structural components of the laboratory, the neutron source and collimator assembly in which it resides, the assembly that represents cargo of given characteristics, a target of highly-enriched uranium (HEU) and large external plastic scintillators for photon detection. The ability of this model to reproduce experimental measurements was tested by comparing simulations with measurements of the number of induced fissions and the number of detected photons when the HUE target was irradiated with 14.25-MeV neutrons in the absence of any cargo and while embedded in assemblies of plywood and iron pipes. The simulations agreed with experimental measurements within a factor of about 2 for irradiation of the bare target and when the areal density of intervening cargo was 33 g cm^{-2} (wood) and 61 g cm^{-2} (steel pipes). This suggests that the model can permit exploration of a large range in parameter space with reasonable fidelity.

1. Introduction

The detection of fissionable material that might be hidden in large seagoing (intermodal) containers has been recognized as a critical problem for national security. Because of their large size (~ 2.5m x 2.5 m x 6-12m) and contents (up to ~ 27 metric tones), this problem represents one of the most challenging environments for development of a detection scheme. For example, when a target is located at the center of a homogeneously-filled container at maximum capacity, the areal density between the target and the container wall is about 75 g cm^{-2}. Given ambient background, detection of either HEU or weapons-grade

1. Department of Nuclear Engineering, University of California, Berkeley California 94708

* Corresponding author. Tel.: +1 925 423 4226; fax: +1 925 423 2795.

E-mail address: prussin@berkeley.edu.

plutonium by passive means in short times is unlikely. Active interrogation to produce and detect a unique signature of these materials appears to be necessary.

We have chosen to examine a methodology based on the use of neutrons in the energy range 2.5 - 14 MeV as the interrogating radiation and the detection of β-delayed γ rays as the signature representing fission. The practical considerations that lead to this choice are discussed in [1, 2] and the principal characteristics of neutron and photon transport in cargos of different types are considered in some detail in [3]. Briefly, cargos can be broadly characterized as moderating or non-moderating with respect to neutron transport, the moderating cargos being hydrogenous, i.e., wood, foodstuffs, plastics, etc., for all practical purposes. Cargos with little or no hydrogen are non-moderating in character. Moderating cargos attenuate fast neutrons relatively well and, because of the high capture cross section of ^{1}H, absorb the thermalized neutrons with high efficiency. Qualitatively, only those fast neutrons reaching the target or thermalized in its vicinity are effective for producing fission. In non-hydrogenous cargos, such as metals, the scattering cross sections and the energy loss per scattering are sufficiently small that essentially no thermalization takes place before the average neutron escapes from the container.

Contrary to what is found with neutrons, all cargos attenuate photons with roughly the same attenuation coefficients, expressed in units of $cm^2\ g^{-1}$, for photons with energies in the range $2 \le E_\gamma \le 6$ MeV [4]. This arises because of the dominance of incoherent scattering in this energy range. At 3 MeV, for example, attenuation cross sections are typically about 0.035 $cm^{-2}\ g^{-1}$ and the fraction of such photons that emerge uncollided after penetrating a thickness of 75 g cm^{-2} is about 0.07. It is because of this high penetrability, compared to the penetrability of characteristic β-delayed neutrons in hydrogenous cargos, the relatively high yield of such γ rays in decay of the short-lived fission products ($0.5\ s \le t_{1/2} \le 250\ s$) and their unique time dependence that this signal was selected as the signature of fission [1, 2].

The number of possible cargo and target configurations is obviously very large and will include both homogeneous and heterogeneous configurations. The only reasonable means to explore interesting cases with high confidence in such a large space is to develop a Monte Carlo model with sufficient detail to simulate experimental arrangements with high reliability. In this paper we present a model developed for this purpose and compare its predictions to the results from three different experiments made with a 14.25-MeV neutrons; irradiation of a bare HEU target, irradiation of the target embedded in plywood and irradiation of the target embedded in an array of steel pipes, the latter two arrangements being reasonably representative of hydrogenous and non-hydrogenous cargos. Because of the high-energy of the neutrons, large quantities of ^{16}N were produced via the reaction $^{16}O(n,p)^{16}N$ that seriously limited the sensitivity for observing a delayed γ-ray signal. ^{16}N has a half life of 7.13 ± 0.02 s and an intense 6.129-MeV γ ray [5]. Its presence strongly interferes with the delayed γ-ray signal and thus provides a very stringent test of the ability of the model and data analysis procedures to describe experiment.

2. The Monte Carlo Model

The laboratory in which the experiments were performed is a large highbay structure with a room (pit) below the main floor in which the neutron generator and its housing

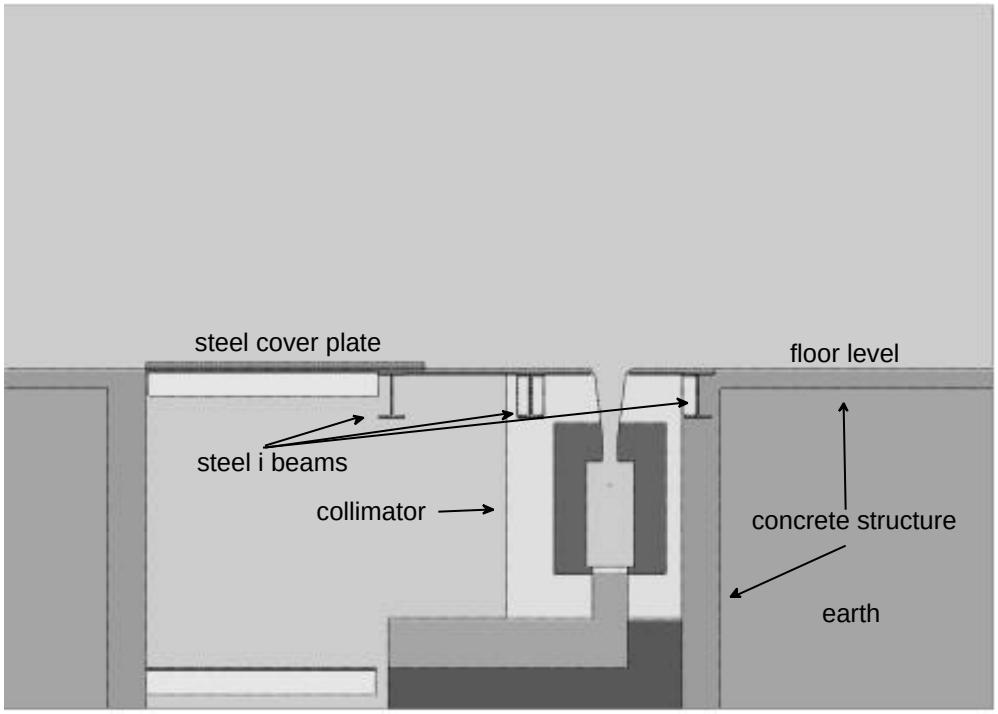

Figure 1. Schematic of the laboratory construction contained in the Monte Carlo model.

were situated.The model developed for the Monte Carlo simulations contains the principal components of the structure shown schematically in Figure 1 and the details of the pit and generator housing (collimator) shown in Figure 2. The model includes the concrete floor and walls of the pit and the earth below it. The collimator is constructed of steel plates, to provide relatively rapid reduction of neutron energy, and is surrounded by polyethylene to further moderate and to absorb thermal neutrons. The opening in the collimator through which neutrons emanate for irradiation of target assemblies has dimensions of 30.5 cm x 30.5 cm. The collimator structure and its support were modeled as continuous segments of the various materials of their construction with their actual physical dimensions and generic compositions.

The DT neutron generator used here was a refurbished Kaman Nuclear device [6]. The neutron source was modeled as a cylindrical (0.635 cm (dia) x 0.254 cm (thickness)) isotropic source of 14.25-MeV neutrons located in the collimator at 92.7 cm below the floor of the laboratory.

Four detectors were used for measurements of γ-ray spectra, two with dimensions of 61 cm x 122 cm x 15 cm and two with dimensions of 61 cm x 61 cm x 15 cm. The four

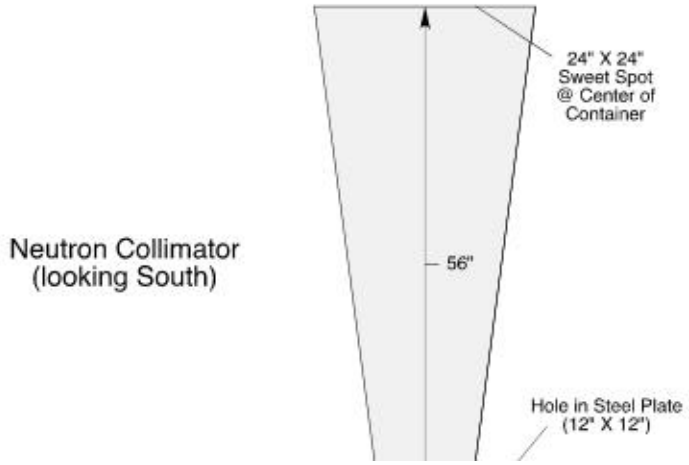

Figure 2. Details of the collimator housing for the neutron generator. The location of the (d,t) target is shown as the partially-shaded circle. In the present experiments, the Pb plug shown in the throat of the steel structure was not present.

Figure 3. The array of plastic detectors in their light-steel support (to the left) along with the assembly of plywood (to the center and right).

detectors were mounted in a light steel support structure as shown in Figure 3. The detectors were plastic scintillators with the nominal composition of C_9H_{10} and were obtained form Eljen, Inc. [7]. The larger detectors were viewed by two 20.3-cm (dia) phototubes separated by 30.5 cm and symmetrically centered about the centerline of the upper 30.5 cm x 15 cm face of the detector. The smaller detectors were viewed by single phototubes of the same dimension centered on the back 30.5 cm x 30.5 cm face of the detector. The detectors were modeled as individual entities along with the support structure, all at nominal densities and chemical compositions.

The mock hydrogenous cargo was constructed from common plywood with dimensions of 244 cm x 122 cm x 183 cm (Figure 3). Monte Carlo calculations showed that this assembly produced essentially the same neutron intensity and energy spectrum at its center as that expected in a fully loaded cargo container of the same density and composition. Samples of the plywood were analyzed for density and composition and these parameters (Table 1) were used in the model.

Table 1. Characteristics of the plywood used as mock hydrogenous cargo.

Property	Mean Value	Error (%)
density (g cm^3)	0.55	10.0
composition (wt. %)		
carbon	48.38	0.3
oxygen	44.99	0.1
hydrogen	6.43	0.3
nitrogen	0.06	0.01
sulfur	0.02	0.01
water	6.76	0.02
ash	1.00	0.02

The mock cargo of non-moderating type was a 244 cm x 183 cm x 122 cm array of steel pipe with outer diameter of 8.89 cm and 0.55 cm in thickness. Close packed layers of the pipe were separated by rectangular spacers to provide an average density of 0.6 g cm^{-3}, the maximum average density allowed by the weight limits of a standard cargo container. Monte Carlo simulations demonstrated that this assembly produce essentially the same neutron intensity and spectrum at its center as a homogenous assembly of iron at a density of 0.6 g cm^{-3} that completely filled a cargo container. A photograph of the assembly is shown in Figure 4.

Two HEU targets in the form of U_3O_8 were used in the experiments and their characteristics are given in Table 2. The targets were doubly encapsulated in identical cylindrical steel containers and the inside diameter of the inner container was 8.6 cm. The targets were modeled as uniform cylindrical slabs with heights of 2.61 cm and 3.34 cm, respectively, and the steel containers were modeled as ideal cylindrical containers of actual thickness and nominal composition.

Table 2. Characteristics of HEU targets used in the experiments

Target	Mean Density (g cm^{-3})	Total Mass (g)	Mass of U (g)	Abundance of 235U (at %)
large	2.4	469.7	397.6	94.69
small	2.4	280.4	237.3	93.17

Figure 4. The array of steel pipes that represents a cargo container filled homogeneously with steel at a density of 0.6 g cm^{-3}. The axes of the pipes in a given layer ar orthogonal to those in adjacent layers. The ends of the roughly square spacers are clearly sees between the layers of pipe.

The model was encoded for the LLNL 3D Monte Carlo particle transport code COG [8]. Simulations used standard ENDF/BVIR7 libraries for photon and neutron transport and a newly-developed module [9, 10] for the time- and energy-dependent emission of β-delayed γ rays. This module incorporates the nuclide and decay properties contained in the NUDAT data files [11] and the fission yields of England and Rider contained in ENDF/BVI [12]. To minimize the time required for computations of good statistical quality, the transport problem was separated into two parts. In the first, source neutrons were transported to simulate the number of fissions produced in a target per source neutron. In the second, photons were transported to simulate the average fluence of photons incident on the plastic detectors per fission. Only delayed γ rays with source energies $E_\gamma \geq 1.5$ MeV were transported. The production of activation products and transport of reaction and decay photons were not simulated. To compare with experimental photon spectra, the simulated fluence of the delayed γ rays was converted into a detected spectrum using the response function described in ref. [13] outside of the COG code.

As discussed above, the neutron spectrum incident on the HEU target may be strongly dependent on the presence and character of the medium in which the target is

embedded. To illustrate the spectra expected for the three experiments considered here, schematic simulations were performed to estimate the neutron spectra incident on the target in the absence of cargo and with the target embedded in the plywood and steel assemblies. These spectra are shown in Figure 5. Each of the spectra exhibits a characteristic

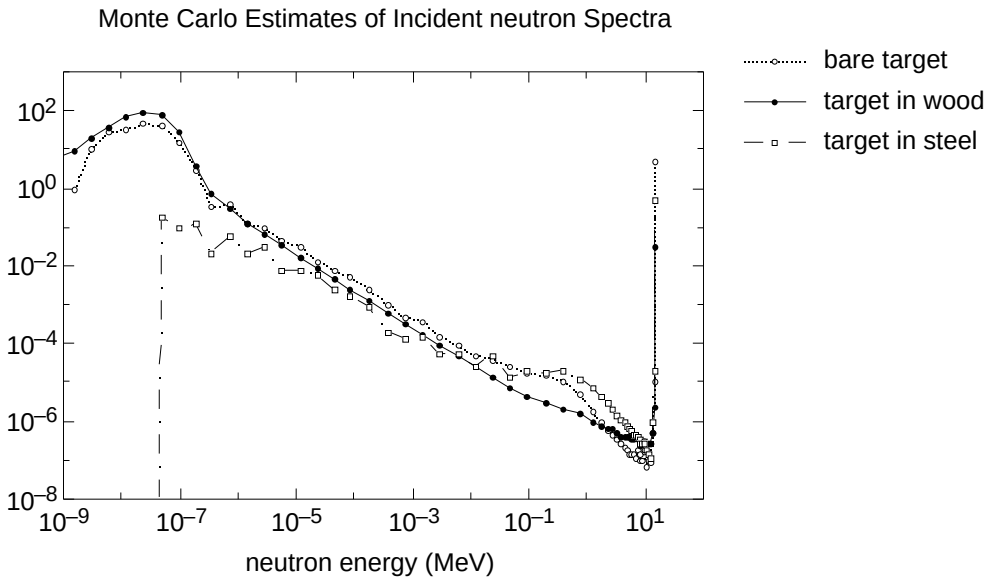

Figure 5. Simulated neutron spectra incident upon the large HEU target in the absence of cargo (open circle plus dotted line) and when embedded in the wood (closed circle and solid line) and plywood (open squares plus dot-dashed lines) assemblies. In each case, the target was located on the axis of the beam and at a height of 188 cm above the laboratory floor in the presence of a 2.54-cm thick steel plate. When present, the thicknesses of the intervening cargo was 68 g cm^{-2} (wood) or 70.6 g cm^{-2} (steel pipe).

1/E energy dependence in the range of 10^{-6} - 0.1 MeV. When no cargo is present, the spectrum is the sum of the direct 14.25 MeV flux emanating through the collimator opening and the flux of lower-energy neutrons that have suffered one or more interactions in the iron and polyethylene of the collimator before escape. In the presence of the wood, the thermal flux at the target is larger in intensity, but the flux at the source energy is reduced by more than two orders of magnitude. With the steel cargo, both the thermal flux and the flux near the source energy are drastically reduced in comparison to the flux emanating from the collimator opening in the absence of cargo. Because of the very strong dependence of the fission cross section on neutron energy, large differences in the fission rates per source neutron can be expected. In Table 3 we show the estimates of the total fission rates per source neutron estimated from the simulations along with the relative contribution of different energy groups to the total. Owing to the very low thermal flux emanating from the collimator, the majority of the fissions produced in the bare target are due to neutrons near the source energy.

Table 3. Total fission rates per source neutron and the contribution from 7 energy groups to the total for the simulations summarized in Figure 5.

	target configuration		
	bare	in wood	in steel pipes
fissions per source neutron	8.40×10^{-6}	6.50×10^{-6}	1.85×10^{-6}
energy range (MeV	Contribution to total fission rate (%)		
10^{-11} - 4×10^{-7}	2.85	36.47	0.06
4×10^{-7} - 10^{-4}	1.15	5.55	0.78
10^{-4} - 1	8.76	18.95	29.82
1 - 14.25	8.76	35.52	50.03
14.25	78.53	3.50	19.31

When the target is embedded in wood, the predicted flux at the source energy is strongly reduced and that at thermal energies is strongly increased. Nevertheless, more than half of the fissions are still due to neutrons with energies greater than about 10^{-4} MeV, primarily because of the removal of thermal neutrons by capture in hydrogen. Finally in steel, a negligible fraction of the fissions are due to low-energy neutrons because thermalization simply doesn't occur to any significant extent. Notwithstanding some differences between the actual experimental arrangements discussed below and those assumed in the simulations, the latter make it clear that it is primarily the high penetrability of the source neutrons that is responsible for significant fission rates at large depths into a cargo.

It is important to point out that computed and experimental fission rates can be quite sensitive to the magnitude of the thermal neutron flux in the vicinity of a target. This arises because of the large fission cross section for thermal neutrons, ~ 580b, as compared to about 5b for 14-MeV neutrons. In hydrogenous materials, the thermal flux will be strongly dependent on the atom density of hydrogen because of the significant thermal absorption cross section of hydrogen. ~0.33b. In addition to the materials of construction included in the model, there are a number of structures in the laboratory that have not been included that could affect the magnitude and shape of the neutron spectrum incident on a target or cargo assembly. Simulations with fairly massive structures added to the problem have shown that the fission rates are rather insensitive to these. Apart from possible errors in neutron cross sections, expected to be small, the results of the neutron transport calculations will depend primarily on the source characteristics, the characteristics of the collimator and the properties of the cargo.

3. Experimental

A detailed description of the experimental apparatus and procedures is given in [14]. In the following, we give a brief description of those aspects important to understanding the comparison of experimental and simulated results, including experimental errors.

The neutron generator provided a maximum output of ~ 4 x 10^{10} n s^{-1} at a nominal energy of 14.25 MeV. To acquire data of sufficient statistical quality, an experiment was performed with a regimen of 10-50 cycles of a 30-s irradiation period followed by 100-s counting interval. The output of the neutron generator was monitored continuously with a small plastic scintillation detector, the generator monitor, that was itself calibrated against an absolute rate measurement with a de Pangher long counter (see ref. 15 and references therein). Small corrections for the presence of scattered neutrons in the beam was accomplished through Monte Carlo simulations.

Signals from γ-ray interactions in the large plastic scintillators were digitized and stored with an MPA-3 multichannel analyzer system that also recorded the output from the neutron generator monitor [16]. The data were collected as successive 1-s spectra summed over all cycles of an experiment.

The signals from the plastic scintillators are dominated by single- and multiple-incoherent scattering events with negligible intensity from total energy absorption for incident photon energies of $E \geq 1$ MeV. As a result, energy calibration was accomplished with the centroid of the broad peaks in the vicinity of the Compton edges in photon spectra from decay of ^{88}Y (898 keV and 1836 keV), ^{40}K (1461 keV), ^{208}Tl (2614 keV) and ^{16}N (6129 keV). These peaks were assigned energies of ($E\gamma - m_e c^2/4$) based on the smoothing of Monte Carlo simulations of such spectra with a detector response function. The uncertainty in the energy calibration obtained in this manner is estimated to be about 0.1 MeV ($\pm$ 1 σ).

4. Results and Data Analysis

4.1 γ-ray Spectra

The total γ-ray spectrum recorded in one of the 61 cm x 122 cm x 15 cm scintillators[2] from irradiation of the small bare HEU target is shown in Figure 6. The spectrum represents the sum of all 1-s spectra over the time range 6 s ≤ t_d ≤ 100 s from a total of ten cycles. Data from shorter decay times were excluded because of the intense ^{16}N induced in the coolant water of the neutron generator by the ^{16}O(n,p) reaction. The flow of the coolant produced a moving source that resulted in a rather complicated time dependence of the signal from the ^{16}N seem in the detector at short times after the end of irradiation.

2. The γ-ray spectra presented in this manuscript were all recorded with this detector.

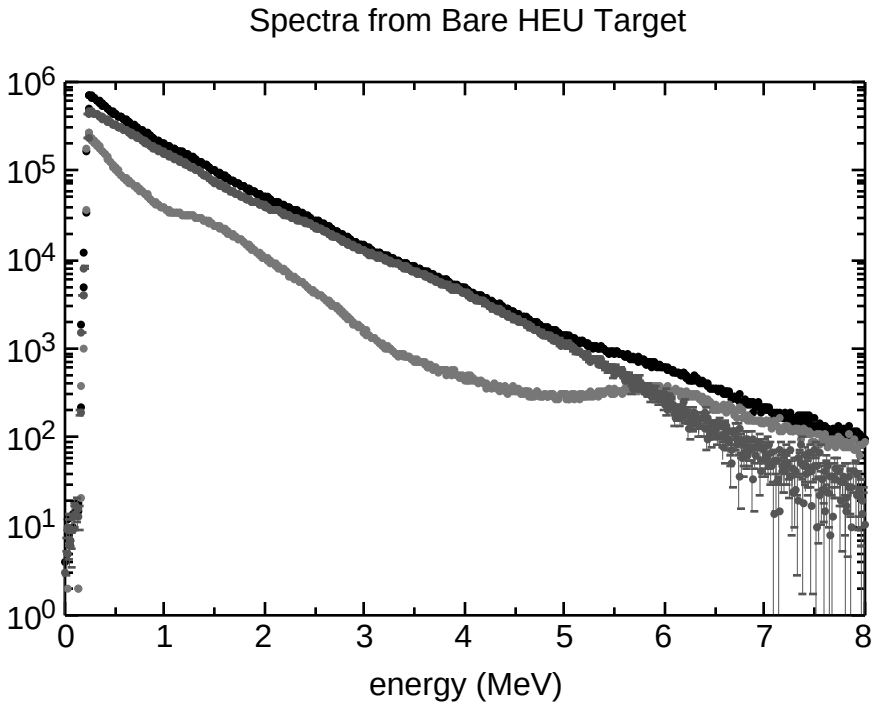

Figure 6. Spectra from irradiation of the small HEU target in the absence of mock cargos. The data have been summed over the counting interval 6 s ≤ t ≤ 100 s and over the ten cycles of irradiation: total spectrum (black), active background normalized by the total counts in the neutron generator monitor (light grey), net spectrum from HEU target (dark grey with error bars).

To obtain a spectrum representative of the decay of activity induced only in the target, a ten-cycle irradiation was performed under exactly the same experimental conditions but in the absence of the target. This "active background" spectrum (light grey in Figure 6) is dominated by signals from the decay of ^{40}K and ^{208}Tl (shoulders near 1.5 and 2.6 MeV) in the natural background and from the decay of ^{16}N induced by neutron irradiation of environmental oxygen (peak near 6.0 MeV). A small contribution is also present from the decay of ^{56}Mn induced in structural iron and the iron and manganese impurities in the concrete and other structures in the laboratory. Experience has shown that no other activities contribute significantly to the active background. In particularly, there is no evidence for the presence of significant activity with a half life $t_{1/2} \leq 10$ min.

Subtraction of the active background spectrum after normalizing by the total counts registered in the neutron generator monitor yields the net spectrum ascribed to the delayed γ rays from the fission products (dark grey with error bars in Figure 6). At energies above about 3 MeV, the spectrum represents the superposition of the decay of some 23 different nuclides that emit a large number of relatively weak γ rays (typically $10^{-3} \leq I_\gamma \leq 10^{-2}$ per fission) with energies extending to about 6 MeV. Coupled with the relatively poor detector resolution, the delayed γ-ray spectrum is seen to be quasi-exponential in character

and diminishes with an energy constant of ~ 1.3 MeV^{-1}. The weak intensity extending above 6 MeV is due primarily to analog summing of signals prior to digitization.

The decay of the raw data in the time range 7 s ≤ t_d ≤ 100 s and energy range 3 MeV ≤ E ≤ 6 MeV is shown in Figure 7. The principal nuclides contributing to the delayed

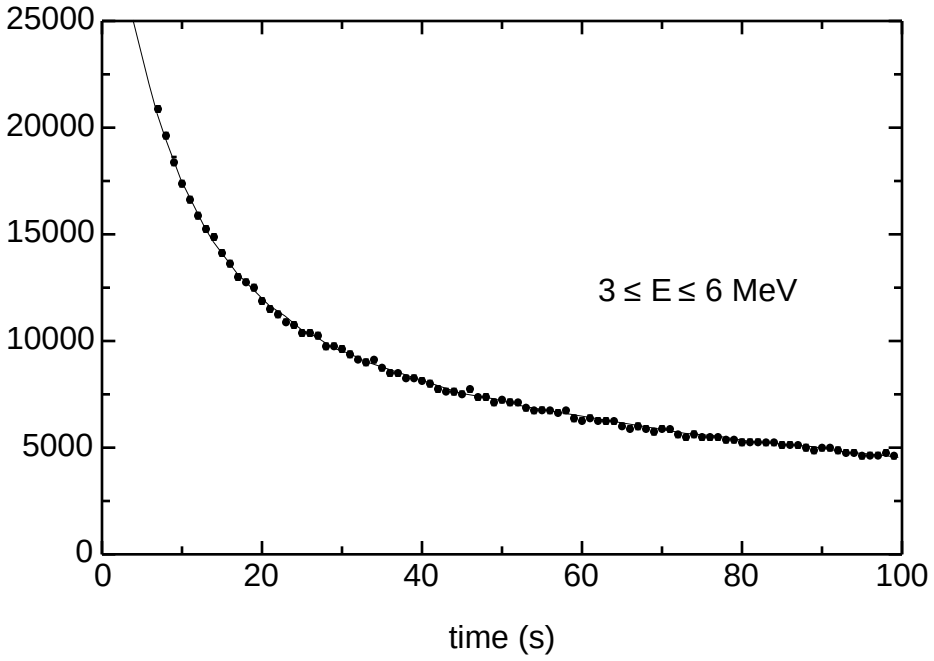

Figure 7. Decay of the signal registered in the plastic scintillator during the period 7 s ≤ t ≤ 100 s following the end of irradiations. The energy range over which data was integrated was 3 ≤ E_d ≤ 6 MeV.

γ-ray spectrum have half lives in the range 0.5 s ≤ $t_{1/2}$ ≤ 258 s. But for the irradiation and counting conditions used in the present experiment, the composite decay during the time range 6 s ≤ t_d ≤ 100 s is well approximated by the sum of three exponential terms. The solid line shown in Figure 7 represents a fit to the decay of the raw data using this representation for the delayed γ rays, a component of fixed decay constant representing ^{16}N and a constant representing ambient background and long-lived activation products. The overall fit is quite good although the residuals between the data and the fitted function show that the latter contains slightly too large a component at short times. The coefficients representing the contributions from ^{16}N and the residual background are quite close to those shown in Figure 6 that were estimated independently from the experimental parameters.

The total spectrum from the irradiation of the large HEU target embedded in the plywood is shown in Figure 8 along with the spectrum from the active background and the

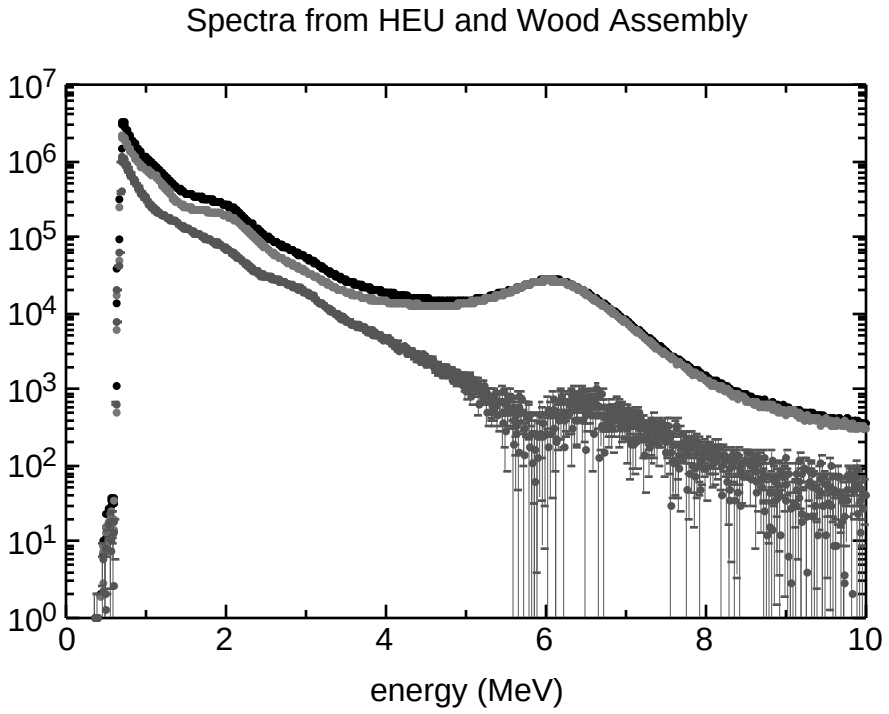

Figure 8. Spectrum from irradiation of the large HEU target embedded in the plywood assembly integrated over the time range 6 s ≤ t ≤ 100 s following the end of irradiations and summed over 50 cycles of irradiation/counting: raw data (black), normalized spectrum from irradiation of the wood assembly in the absence of the HEU target (light grey), net spectrum from the target (grey with error bars).

net spectrum from the delayed γ rays. Immediately evident are the very strong signals from decay of ^{16}N from activation of the high oxygen content of the wood and ^{56}Mn activity from the steel support structure of the plywood. ^{16}N will be an important activation product in the majority of hydrogenous cargos so long as the maximum energy of the neutron source is greater than about 10 MeV and ^{56}Mn will always be present because of the steel construction of the cargo containers considered here. Their combined strength poses a significant challenge when attempting to obtain a net signal from the delayed γ rays by subtracting of the normalized active background. The structure seen in the net spectrum above about 5.8 MeV is likely due to small discrepancies in the energy calibration of the total and active background spectra and differences in spectral shapes due to analog summing of signals prior to pulse-height analysis. Nevertheless, the quasi-exponential spectrum expected from the delayed γ rays is clearly evident below about 5 MeV and it diminishes with about the same energy constant as found in the HEU spectrum from the irradiation of the bare target.

Finally, the total spectrum from irradiation of the large HEU target embedded in the steel pipe assembly is shown in Figure 9 along with those of the normalized active background and the net spectrum. The active background is now dominated by decay of

^{56}Mn with but a small contribution from ^{16}N. But taken together, these two sources clearly represent almost all of the data acquired and the accurate estimation of the contribution from the delayed γ rays by subtraction of active background from the raw data will clearly be very difficult. Indeed, the delayed γ-ray spectrum found in this way is clearly suspect and still contains a significant contribution from ^{56}Mn.

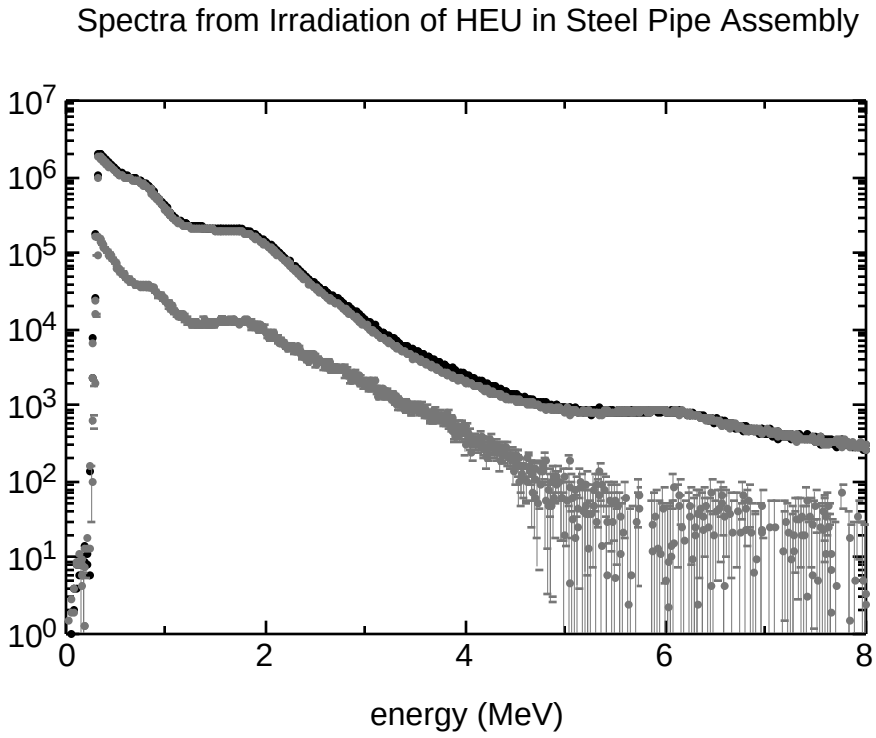

Figure 9. Spectra associated with the irradiation of the large HEU target embedded in the steel pipe assembly. The data were integrated over the time range 6 s ≤ t ≤ 100 s following the end of irradiations and summed over 50 cycles of irradiation/counting.; raw data (black), normalized spectrum from irradiation of the steel pipe assembly in the absence of the HEU target (light grey), net spectrum from the HEU target (grey with error bars).

4.2 Comparison of Experimental and Simulated Fission Rates

The total number of fissions induced in a target was determined by assay of the intensity of the 1024.3-keV and 1383.93-keV transitions in the decay of ^{91,92}Sr, respectively, with a calibrated HPGe detector. Absolute photon intensities and fission yields for the se nuclides were taken from [5] and [12], respectively. The detector efficiency was corrected for photon attenuation in the target with a combination of Monte Carlo simulations and experimental measurements. Fission rates per source neutron were calculated from the expression

$$(R_f)_{exp} = \frac{n_f}{n_n}, \quad (1)$$

where n_f is the average number of fissions estimated from the $^{91,92}Sr$ measurements and n_n is the number of source neutrons obtained from the calibration of the neutron generator monitor count rate. These fission rates for irradiation of the small bare target and the irradiation of the large target embedded in the plywood and steel pipe assemblies are compared to the fission rates obtained directly from the Monte Carlo simulations in Table 4.

Table 4. Comparison of experimental and simulated fission rates. Statistical uncertainties in the Monte Carlo simulations are ≤ 2% and the uncertainties in the cross sections used in the simulations are also small.

target	$(R_f)_{exp}$ sn^{-1}	$(R_f)_{sim}$ sn^{-1}	$\frac{(R_f)_{exp}}{(R_f)_{sim}}$
HEU-bare	$(1.32\pm0.19) \times 10^{-4}$	1.90×10^{-4}	0.69±0.10
HEU-wood	$(1.98\pm0.29) \times 10^{-5}$	3.13×10^{-5}	0.63±0.09
HEU-steel	$(2.15\pm0.30) \times 10^{-6}$	2.20×10^{-6}	1.02±0.14

The principal contributor to the uncertainty in $(R_f)_{exp}$ is the uncertainty in the calibration of the neutron generator monitor. As seen from the last column of the table, the simulated fission rate is within ±1σ of that found in experiment for the irradiation of the HEU in the steel pipe assembly. But when the target was bare or embedded in the plywood, the simulated fission rates were larger than found in experiment by a factor of about 1.5, or about 3.7 σ. In these two cases, the fission rate is sensitive to the magnitude of the thermal neutron flux and even very small discrepancies in the calculated thermal flux emanating from the collimator opening (bare target) or the hydrogen content of the plywood (target embedded in plywood) could easily account for the poorer agreement with experiment.

4.3 Comparison of Experimental and Simulated Photon Fluences

Methodology

The contribution of delayed γ rays to the total spectrum from irradiation of the bare HEU target (Figure 5) is so large that, as shown above, simple subtraction of the active background provides data of sufficient reliability for comparison with Monte Carlo simulations. On the other hand, the contributions of delayed γ rays to the total spectra from irradiation of the HEU target embedded in the plywood and the steel pipe assemblies (Figures 7 and 8) are so weak that even small experimental uncertainties can make the background subtraction technique unreliable.

In an attempt to minimize effects from experimental uncertainties, the intensities of delayed γ-rays were estimated with two approaches that rely on least squares fitting of

the decay of the total γ-ray spectra. The first method (Method 1) was the straight-forward fitting of the time dependence of the spectra in various energy ranges using the relation

$$c(t) = a_1 \sum_{i=1}^{3} b_i e^{-\lambda_i t} + a_2 e^{-\lambda_{16} t} + a_3 . \qquad (2)$$

Here c(t) represents the total counts registered in an energy interval as a function of decay time, $\sum_{i=1}^{3} b_i e^{-\lambda_i t}$ represents the three-component representation of the decay of the delayed γ rays under the repeated irradiation/decay sequences used in each experiment, and a_1, a_2 and a_3 represent the counts at t = 0 from decay of the delayed γ rays, ^{16}N and the sum of the ambient background and long-lived activation products, respectively. Inclusion of an additional decay component with a decay constant as a free parameter in the fitting function did not significantly change the resulting value of any of the a_i. Within the model for the delayed γ rays, the coefficients and decay constants for the three-component representation are not significantly different for the 10- or 50-cycle irradiations and the parameters for the 50-cycles fit are shown in Table 5.

Table 5. Parameters of the three -exponential fit to the delayed γ rays for the 50-cycle irradiation.

i	b_1	λ_i (s^{-1})
1	5.4957×10^{-4}	1.9300×10^{-1}
2	3.6709×10^{-4}	6.0823×10^{-2}
3	5.2655×10^{-4}	9.1223×10^{-3}

In the second method (Method 2), a normalized detected spectrum for each component in a fit is considered as a surface that incorporates the full time- and energy-dependence of the component for the specific irradiation and counting conditions of an experiment. With this representation, the total detected spectrum in energy and time, $c'(E, t)$, is given by

$$c'(E, t) = \sum_{i=1}^{i=4} a_i' g_i(E, t) , \qquad (3)$$

where the $g_i(E, t)$ represent the spectra from delayed γ rays, ^{16}N, ^{56}Mn and all other background, respectively, and the a_i' have the same meaning as in equation (2). Because of its long half life (~ 2.6hr), the time dependence of ^{56}Mn was actually neglected in the fits. Numerical approximations to the surfaces representing the first three components were generated by transporting the photons emitted by each component through a schematic cargo and then applying the detector response function to the resultant spectra incident on

a detector. This method of analysis, while in principle more accurate because it makes use of the energy and time dependence of the various signals in entirety, is more sensitive to uncertainties in the detector response function and pulse summing effects than Method 1.

Experimental and Simulated Photon Intensities for the Bare Target

To compare the experimental data with model predictions for source photons with energies $E_\gamma \geq 1.5$ MeV, the net delayed γ-ray spectrum shown in Figure 5 was converted into an average incident photon fluence per fission incident on a detector by use of the relation

$$(flu)_{exp} = \frac{\int_{1.5}^{6} sp(E)dE}{\langle eff \rangle A n_f \int_{1.5}^{6} flu_{MC}(E)R(E)dE \Big/ \int_{1.5}^{6} flu_{MC}(E)dE} \text{ cm}^{-2} \text{ fiss}^{-1}. \quad (4)$$

Here $\int_{1.5}^{6} sp(E)dE$ is the total intensity in the experimental spectrum over the energy range 1.5 - 6 MeV, <eff> is the average fraction of incident photons that interact with the detector as found from analysis of the Monte Carlo simulation (0.52), A is the area of the detector, n_f is the number of fissions found from analysis of the decay of ^{91,92}Sr ($1.77 \pm 0.11 \times 10^9$), and the ratio $\int_{1.5}^{6} flu_{MC}(E)R(E)dE \Big/ \int_{1.5}^{6} flu_{MC}(E)dE$, where $flu_{MC}(E)$ is the fluence per fission estimated from the Monte Carlo simulations and R(E) is the response function of the detector, represents the fraction of incident photons that result in energy depositions with energies $E \geq 1.5$ MeV (0.38). The average incident photon fluence per fission calculated in this way for the single detector considered here was found to be $(1.95 \pm 0.53) \times 10^{-6}$ cm^{-2}fiss^{-1}. The uncertainty represents contributions from the uncertainties in each of the parameters in equation (4) and rough estimates of the uncertainties in fission yields and the absolute yields of the delayed γ rays. The corresponding fluence produced directly in the Monte Carlo simulation was 1.08×10^{-6} cm^{-2}fiss^{-1} with a statistical uncertainty of about 3%. The experimental fluence agrees with the simulation within about 2σ.

Ratios of experimental fluences per fission for the three experiments considered here and for the two analysis procedures discussed above are given in Table 6 for the cases where Method 1 was applied to the energy range 4.1 - 5.5 MeV (second column) and Method 2 to the energy range 1.5 - 6.0 MeV (fourth column). The corresponding ratios from the Monte Carlo simulations are given in the third and fifth columns, respectively. The data imply that the delayed γ-ray intensities extracted by both methods when the HEU target was imbedded in the wood or steel pipe assembly are within about ± 2σ of those

estimated from the Monte Carlo simulations, the detector response function and the experimental measurements of the number of fission produced in each experiment. Although not included here, the ratios found from Method 1 for other energy ranges above 2.5 MeV were similar to those shown in the table.

Table 6. Relative intensities of detected delayed γ rays compared to predictions from Monte Carlo simulations, detector efficiencies and measured number of fissions.

target	$a_{1,4.1\text{-}5.5}$ (rel.)	$flu_{4.1\text{-}5.5}$ (rel.)	$a'_{1,1.5\text{-}6.0}$ (rel.)	$flu_{1.5\text{-}6.0}$ (rel.)
HEU-bare	1.00±0.02	1.00±0.25	1.00±0.01	1.00±0.25
HEU-wood	0.203±0.007	0.479±0.120	0.460±0.024	0.447±0.112
HEU-steel	0.0139±0.0033	0.0185±0.0046	0.0334±0.0083	0.0175±0.0044

6. Discussion

The experimental tests of the fission rates and delayed γ-ray signals from HEU targets embedded in thick models of moderating and non-moderating cargos, suggest that the Monte Carlo model is likely to provide quite reasonable simulations of results expected for a wide variety of cargo types. Accounting for the mass difference in the targets used, the 33 g cm^{-2} of plywood and 61 g cm^{-2} of the steel pipes reduced the overall fission rate per source neutron by factors of about 10 and 100, respectively, compared to that of the bare target, while the photon fluences incident upon the detector chosen for study were reduced by factors of about 2 and 50, respectively. As a result, the experiments, which provide data within about a factor of 2 of the simulation results, have provided reasonable first tests of the ability of the Monte Carlo model to account accurately for the spectral changes and intensities that result from the transport of both neutrons and photons.

The principal sources of experimental error lie in the calibration of the neutron source and the detector response function, where systematic errors have not been quantified well, and, because of the near exponential character of the delayed γ-ray spectrum, the energy calibration of the plastic scintillators. On the other hand, the principal source of uncertainty in the Monte Carlo simulations is thought to be the uncertainties in the composition of the materials included in the model. This is especially true of the complex and nonuniform plywood and the concrete of the building structure.

A possible systematic error may be the source of the discrepancies between experiment and simulation in the fission rates for the irradiations of the bare HEU target and when the target was embedded in the plywood assembly. These experiments are very sensitive to the thermal neutron flux at the target position whereas the number of fissions induced in HEU while embedded in the steel pipe assembly is essentially independent of the thermal flux. Initial calibration measurements of the thermal neutron flux emanating

from the collimator opening were performed with a ^{3}He ionization tube. Changes in the configuration of the laboratory from the time of calibrations to the time the present experiments were conducted could have resulted in some changes in the thermal flux.

The experiments reported here have been limited by the relatively low intensity of the 14-MeV source and the attendant production of ^{16}N and ^{56}Mn, both of which interfere strongly with the high-energy signature delayed γ rays, especially the former. Their absence would markedly increase the sensitivity for quantitative assay of a delayed γ-ray signal.The production of ^{16}N and ^{56}Mn is dominated by (n,p) reactions that have effective thresholds (including the effects from the Coulomb barriers) of about 10.5 and 5.5 MeV, respectively. Thus, their production would be eliminated or markedly reduced by use lower-energy neutrons, albeit at a somewhat reduced neutron penetrability into hydrogenous materials. A new accelerator that provides a maximum neutron energy of about 7 MeV has been constructed and is now in use to study the interrogation methodology, to search for other possible interferences and to provide the information needed to optimize a practical system. This will be the subject of future publications on this topic.

References

1. E. B. Norman et al., Nucl. Instrum. Methods Phys. Res. A 521, 608 (2004).
2. D. Slaughter et al., Lawrence Livermore Laboratory Report, UCRL-ID-155315, August 2003 (unpublished).
3. J. Pruet, M.-A. Descalle, J. Hall, B. Pohl and S.G. Prussin, J. Appl. Phys. 97, 094908 (2005).
4. XCOM: Photon Cross Sections Database, M.J. Berger, J.H. Hubbell, S.M. Seltzer, J. Chang, J.S. Coursey, R. Sukumar, and D.S. Zucker, NIST Standard Reference Database 8 (XGAM), http://physics.nist.gov/PhysRefData/Xcom/Text/XCOM.html.
5. R.B. Firestone and L.P Ekstrom, “Table of Radioactive Isotopes”, January 2004 (http://ie.lbl.gov/toi/)
6. Kaman Sciences Corporation, Colorado Springs, Colorado, USA.
7. Eljen Technology, P.O. Box 870, 300 Crane Street, Sweetwater, Texas 79556 (USA).
8. “The COG Code System”, UCRL-MI-123157, 1999, http://www-phys.llnl.gov/N_Div/COG/COG_home.html.
9. J. Pruet, J. Hall, M.-A. Descalle and S. Prussin, Nucl Instr. and Methods in Phys. Res. B, 222, 403 (2004).
10. J. Hall, J. Pruet, D. Brown, M.-A. Descalle, G. Hedstrom and S. Prussin, "Modeling the production of beta-delayed gamma rays for the detection of special nuclear materials", Lawrence Livermore National Laboratory Report UCRL-TR-209738 (2005), unpublished.
11. National Nuclear Data Center, Brookhaven National Laboratory (USA) (http://www.nndc.bnl.gov/).
12. T.R. England and B.F. Rider, Los Alamos National Laboratory Report, LA-UR-94-3106, October, 1994.
13. D. Petersen et al., to be published.
14. S. Asztalos et al., to be published.

15. D.R. Slaughter and D.W. Rueppel, Nucl. Instr. and Methods 145 (1977) 315.
16. Fast Com Tec GmbH, Gruenwalder Weg 28a, D-82041 Oberhaching, Germany.

This work was performed under the auspices of the U.S. Department of Energy by the University of California, Lawrence Livermore National Laboratory under Contract No. W-7405-Eng--48.